Science and Technology Indonesia
e-ISSN:2580-4391 *p*-ISSN:2580-4405
Vol. 11, No. 3, July 2026

Research Paper

Initial Assessment of a Dual-Bioactive Hydrogel Incorporating Phagocytosis-Stimulating and Tissue-Regenerative Proteins for Enhanced Wound Healing

Papassara Changklang[1], Tan Suwandecha[2*], Somchai Sriwiriyajan[1], Jongdee Nopparat[1], Neelam Balekar[3], Teerapol Srichana[4]

[1]*Division of Health and Applied Sciences, Faculty of Sciences, Prince of Songkla University, Hat Yai, Songkhla, 90110, Thailand*
[2]*School of Pharmacy and Drug and Cosmetic Excellence Center, Walailak University, Thasala, Nakhon Si Thammarat, 80160, Thailand*
[3]*College of Pharmacy, IPS Academy, Indore, Madhya Pradesh, 452012, India*
[4]*Department of Pharmaceutical Technology, Faculty of Pharmaceutical Science, Prince of Songkla University, Hat Yai, Songkhla, 90112, Thailand*
***Corresponding author**: tan.su@wu.ac.th

Abstract
Wound healing is a complex process that can be impaired by various factors. Hydrogel is a recommended choice for keeping the skin moist and enhancing wound healing. Hydrogel can contain bioactive compounds to improve wound healing effectiveness further. Phagocytosis activating protein (PAP) and thrombospondin (TSP) can stimulate macrophages and promote cell proliferation. They had the potential to enhance wound healing when incorporated into a hydrogel. This study aims to evaluate the effects of PAP and TSP hydrogels on skin irritation and wound healing efficacy in a rat model. This experiment is conducted using a full-thickness wound model in rats. The hydrogel formulations with PAP and/or TSP were applied to the wounds for 21 days. The wound contraction, histology, and TGF-β1 expression were measured. The results showed that low-dose PAP hydrogel had the best wound healing performance among all groups (95% contraction), with high TGF-β1 positive cells in the early phase (14.95 ± 0.64%) and low levels in the late phase (7.12 ± 0.75%). Low-dose TSP hydrogel had similar but weaker effects than low-dose PAP hydrogel. There was no sign of skin irritation for all formulations. Hydrogel containing a low dose of PAP or TSP is a promising formula for further developing new wound dressing materials. It also opens an opportunity to cure some challenging-to-treat wounds, such as diabetic and burn wounds.

Keywords
Wound Healing, Phagocytosis Activating Protein, Thrombospondin, Hydrogel

Received: 7 March 2026, Accepted: 31 May 2026
https://doi.org/10.26554/sti.2026.11.3.1127-1137

1. INTRODUCTION

Biomaterial-based therapies have received considerable attention in tissue regeneration and wound care due to their ability to replicate the extracellular matrix, creating an optimal environment for cell growth and proliferation (Acciaretti et al., 2022; Zhao et al., 2022). Hydrogels have become a major focus because of their high water retention capacity, customizable structures, good biocompatibility, and adjustable mechanical strength. These characteristics make hydrogels effective carriers for bioactive molecules while also maintaining a moist environment that supports tissue repair and regeneration (Sari et al., 2023; Zhao et al., 2022).

A key challenge in wound healing is moving from the inflammatory phase to the proliferative phase. Extended inflammation periods and slow epithelialization often result in chronic wounds or excessive scarring (Ozgok Kangal and Kopitnik, 2026). Thus, effective treatment must suppress early inflammation while also encouraging cell growth and blood vessel formation (Smith and Rai, 2024).

The wound healing process begins with hemostasis, where vasoconstriction and blood clot formation help stop bleeding. Then it is followed by the inflammation phase that is fundamentally driven by macrophage phagocytosis (Ozgok Kangal and Kopitnik, 2026). Macrophages clear cellular debris, pathogens, and apoptotic neutrophils. This process is known as efferocytosis (Sun et al., 2026). Phagocytosis is essential across all stages of wound healing. Macrophages facilitate this process by clearing debris, pathogens, and apoptotic cells. Multiple studies have demonstrated that enhancing macrophage phagocytic activity through glucan-based formulations significantly improves fibroplasia, re-epithelialization, and wound tensile strength (Koh and DiPietro, 2011; Larouche et al., 2018; Zhao et al., 2024). This phagocytic activity also triggers a phenotypic shift in macrophages, prompting them to secrete transforming growth factor-beta 1 (TGF-β1) (Guo and DiPietro, 2010). TGF-β1 is a master regulatory cytokine that signals

the end of inflammation and initiates the proliferative phase by modulating angiogenesis, fibroblast activation, and collagen synthesis (Guo and DiPietro, 2010; Miyazono, 2000). Consequently, enhancing macrophage phagocytic activity has been shown to indirectly accelerate fibroplasia and increase wound tensile strength by amplifying this TGF-β1 signaling cascade (Zhao et al., 2024). TGF-β1 has been identified as a potential biomarker for assessing wound healing progress (Grellner et al., 2005; Miyazono, 2000).

Phagocytosis Activating Protein (PAP) is a critical protein involved in immune modulation and wound healing. It is derived from the phagocytosis activating protein gene and plays a crucial role in stimulating the phagocytic activity of macrophages (Deachamag et al., 2006). Mechanistically, PAP enhances phagocytosis by interacting with the untranslated regions (UTRs) of p53 mRNA, promoting its circularization and thereby optimizing p53 translation (Terzian and Lozano, 2010). This process leads to the activation of the p53/NF-κB pathway, which in turn enhances macrophage activity and promotes immune responses necessary for efficient wound healing (Lowe et al., 2014).

Following the inflammation phase while PAP drives a pro-repair environment, re-epithelialization requires direct mitogenic stimulation. This phase is driven by growth factors, which are essential for the activation and proliferation of fibroblasts, epithelial cells, and endothelial cells. Thrombospondins (TSPs) are a family of glycoproteins that regulate various cellular activities. This study focuses on thrombospondin-3 (TSP-3), which forms a pentameric structure via disulfide linkages. TSP-3 contains an epidermal growth factor (EGF)-like domain that has been shown to induce EGF receptor activation in a dose- and time-dependent manner (Liu et al., 2009).

The activation of EGF receptors promotes cell proliferation, migration, survival, angiogenesis, and resistance to apoptosis, which are key processes in tissue repair (Huang and Fu, 2015). Studies have demonstrated that TSP-3 derived from banana shrimp (*F. merguiensis*) enhances fibroblast proliferation and collagen synthesis, further highlighting its therapeutic potential (Wonglapsuwan et al., 2020).

Previously, mainstream wound healing therapies often relied on single bioactive agents such as recombinant human epidermal growth factor (rhEGF) alone in ointment (Zhang and Liu, 2020) or generalized phagocytosis promoters like glucans (Zhang et al., 2022). However, these single-target therapies have limited effectiveness. Growth factors play little role in inflammatory phases, while phagocytosis promoters alone lack a direct proliferation effect on the epidermis. Thus, there is a growing trend toward multiple bioactive combination approaches to address the complexity of wound healing processes, particularly for chronic wounds (Bogadi et al., 2025; He et al., 2024). Some research has successfully developed effective multiple bioactive combinations such as combinations of basic fibroblast growth factor (bFGF) and heparin, that accelerate skin graft donor site healing (Kohyama et al., 2024) and a hydrogel containing various cytokines and growth factors from umbilical cord mesenchymal stem cell secretome for promoting chronic wound healing (Widowati et al., 2025). Therefore, we propose that co-delivery of PAP and TSP-3 can offer a unique synergistic advantage.

This study preliminarily investigates the in vivo effects of a hydrogel formulation containing two bioactive molecules, PAP and TSP-3. Complete physicochemical characterizations and release-profile studies of hydrogels are not part of the current work at this stage. This research focuses on evaluating the potential application of the formulation in wound healing. Specifically, wound healing efficacy is assessed by macroscopic wound contraction rates, basic histological evaluation of wound tissue, and measurement of TGF-β1 levels as the primary molecular indicator of a successful pro-regenerative transition.

2. EXPERIMENTAL SECTION

2.1 Materials

The materials used in this study included Poloxamer 407, polyvinyl alcohol, glycerol, propanediol, sodium ascorbate, and hyaluronic acid. Pentobarbital sodium was sourced from Ceva Santé Animal (Libourne, France). For immunohistochemical analysis, anti-TGF-β1 MAB240 and the anti-mouse HRP-DAB cell and tissue staining kit were obtained from R&D Systems (MN, USA). Thrombospondin-3 (TSP-3-2) was produced by cloning the TSP3-2 gene from banana shrimp (*Fenneropenaeus merguiensis*) into *E. coli* strain BL21(DE3), following the methodology described by Wonglapsuwan et al. (2020). Similarly, phagocytosis activating protein (PAP) was obtained based on the protocol outlined by Wonglapsuwan et al. (2016).

Table 1. Hydrogel Formulation Containing PAP and TSP

Formulation	PAP (μg/ml)	TSP (μg/ml)
#1 (PL)	0.5	-
#2 (PH)	5.0	-
#3 (TL)	-	1.0
#4 (TH)	-	10.0
#5 (PTL)	0.5	1.0
#6 (PTH)	5.0	10.0

2.2 Preparation of Hydrogel Containing PAP and TSP

A hydrogel base was formulated using Poloxamer 407 (P407), polyvinyl alcohol, sodium borate, and water, following the method described by Kamlungmak et al. (2019). Briefly, P407 (28% w/w) was dispersed in purified water, stirred at 400 rpm on an ice bath for 2 h and stored at 4 °C for 24 h to ensure complete hydration. Separately, PVA (7.14% w/w) was dissolved at 90 °C under constant stirring at 400 rpm for 2 h and stored at 25 °C for 24 h. The cPVA component was formed by cross-linking the PVA solution with sodium borate (0.15% w/w). For the final blend, the P407 and cPVA were blended at an optimal 60:40 ratio. The resulting base formulation exhibited a gelation temperature of 29.7 °C and a viscosity of 23,000 - 24,000 cP , and its final pH was adjusted to 6.5 using sodium

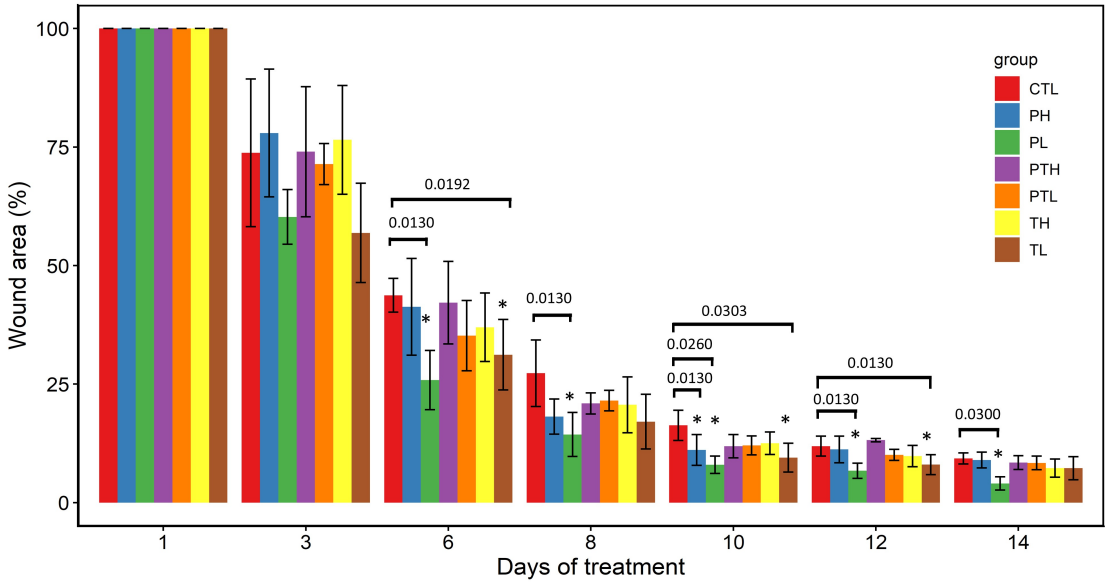

Figure 1. Wound Contraction for All Treatment Groups from the 1st to 14st Day of Treatment. Data are Presented as Mean ± SD (n=6). *p < 0.05 vs Control. Brackets Indicate Adjusted p-Values for Significant Differences Between Treatment Groups and the Control on Specific Days

ascorbate. Either PAP or TSP was then incorporated into the hydrogel base at varying concentrations, as detailed in Table 1 and stored at 5 °C until use.

Dose selection was based on previous studies of the shrimp-derived phagocytosis-activating protein (PAP) (Deachamag et al., 2006) and the thrombospondin EGF-like peptide (TSP3-2) (Wonglapsuwan et al., 2020). In hemocyte assays, a concentration of 0.5 μg/mL of recombinant PAP significantly promoted phagocytic activity (Deachamag et al., 2006). Additionally, systemic administrators of PAP up to 15 μg/g body weight of Penaeus monodon were considered safe and effective (Shekhar et al., 2012). Therefore, concentrations of 0.5 to 1.0 μg/mL of PAP were selected to overcome matrix entrapment, exudate dilution, and proteolytic degradation.

The effective concentration of TSP3-2 for the proliferation of the skin fibroblasts ranged from 0.5-15 μg/mL with an optimal concentration at 0.5 μg/mL (Wonglapsuwan et al., 2020). Accounting for wound exudate and protein degradation at the wound site, concentrations of 1–10 μg/mL of TSP-3 were selected for the hydrogel matrix for the purpose of maintaining continuous optimal therapeutic concentration in the wound environment.

2.3 Experimental Animals and Wound Model

Sprague-Dawley rats (Nomura Siam International Co., Ltd.), aged 8–10 weeks and weighing 200-300 g, were used in this study. The animals were housed under controlled environmental conditions, including 23 ± 2 °C, 55–60%RH, and a 12-hour light/dark cycle. They had free access to a standard pellet diet and water. All experimental protocols were approved by and conducted in accordance with the Institutional Animal Care and Use Committee (IACUC) of Prince of Songkla University. To ensure humane care of laboratory animals, carprofen (5 mg/kg) was administered for pain relief during the first 24 hours. The rats were daily monitored for general behavior, mobility, food and water consumption, and the condition of the surgical site. Any animal exhibiting signs of severe distress, systemic infection, or a rapid weight loss exceeding 20% of its initial body weight was designated for immediate euthanasia.

$$n = \frac{2\left(Z_{1-\alpha/2} + Z_{1-\beta}\right)^2 \cdot \sigma^2}{\Delta^2} \quad (1)$$

n = Sample size
$Z_{1-\alpha/2}$ = 1.96 (for α = 0.05)
$Z_{1-\beta}$ = 0.84 (for 80% power)
Δ = Effect size (difference in means)
σ = Variance

The difference in means of 8.3 and a standard deviation of 10.14 were utilized for the calculation based on data from Aramwit and Sangcakul (2007). The statistical power and significance level were at 80% and σ= 0.05, respectively. The minimum required sample size was determined to be 24 animals. A 25% attrition rate was proactively incorporated into the experimental design. Thus, the sample size was increased to 30 animals.

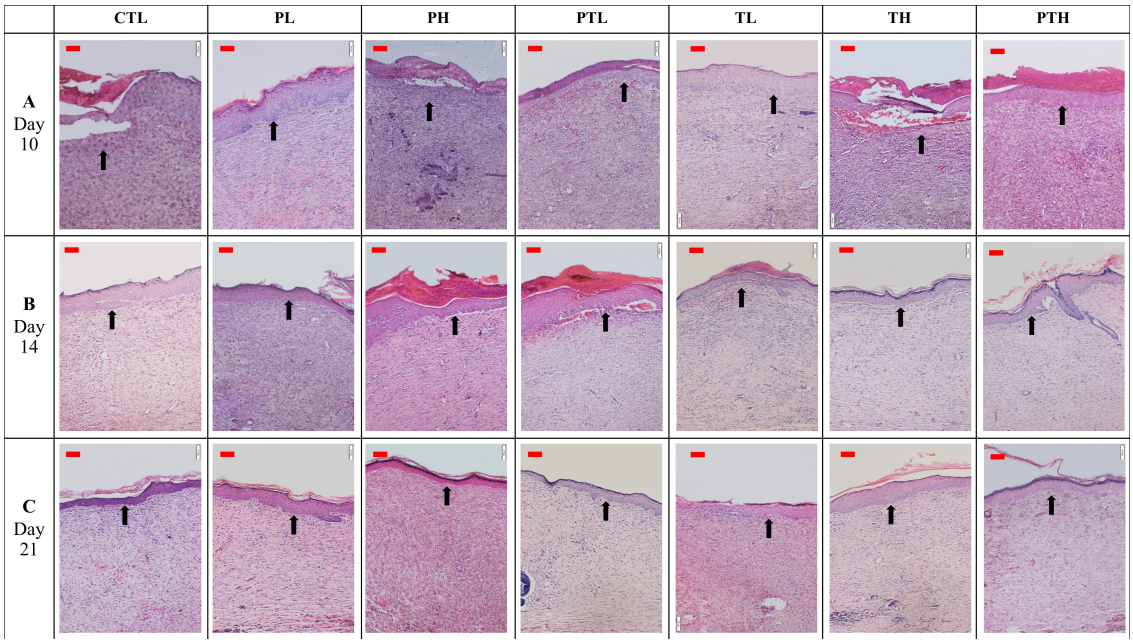

Figure 2. Hematoxylin & Eosin Staining of Histological Sections from Rat Wound Tissue on Days 10 (A), 14 (B), and 21 (C). Arrows Indicate the Epithelial Cell Layer (100× Magnification). Scale Bar = 100 μm

For the surgical procedures, the dorsal hair of the rats was shaved with an electric shaver, and anesthesia was induced with intraperitoneal injection of pentobarbital sodium at a dose of 40 mg/kg. Four distinct, full-thickness excision wounds 8 × 8 mm on the dorsal surface were created using surgical scissors and forceps. This method is a well-established practice in biomaterial research for evaluating topical formulation (Kamlungmak et al., 2021; Mârza et al., 2024). To prevent localized interaction between treatment sites, the wounds were strategically spaced 1.5 cm apart along the dorsal region.

The animals were randomly allocated to two groups using computer-generated randomization. Wounds on each animal received localized applications of different hydrogel formulations:

Group 1: Received PAP low dose (PL) to the upper left wound, PAP high dose to the upper right, PAP/TSP low dose (PTL) to the lower left, and the control hydrogel to the lower right.

Group 2: Received control hydrogel on the upper left wound, TSP low dose (TL) on the upper right, TSP high dose (TH) on the lower left, and PAP/TSP high dose (PTH) on the lower right.

Following hydrogel application, all wounds were covered with transparent film dressing (Opsite® Flexigrid, Smith & Nephew, USA), padded with sterile gauze, and secured with Transpore® surgical tape (3M, USA).

2.4 Wound Contraction Study

Wounds were photographed alongside a ruler on alternating dressing days. The wound area was subsequently measured using ImageJ software. The wound size measurement was an open-label study and performed by three independent evaluators. The wound area reduction was calculated relative to day 1 using Equation (2).

$$\text{Wound area compared with day 1 (\%)} = \frac{\text{Wound area on day n} \times 100}{\text{Wound area on day 1}} \quad (2)$$

2.5 Histological Examination

Histological specimens were harvested on days 1, 10, 14, and 21. The rats were anesthetized with pentobarbital sodium (40 mg/kg) prior to excision of the wound tissues. The collected tissues were fixed in 10% neutral buffered formalin solution, processed in a tissue processor (TP1020, Leica®, Wetzlar, Germany), embedded in paraffin blocks, and sectioned to a thickness of 5 μm. Sections were stained with Hematoxylin and Eosin (H&E) for morphological analysis and examined under an inverted light microscope (Olympus IX73®, Olympus, San Diego, USA).

Histological scoring and image analysis were conducted according to a second-opinion protocol. All slides and digitized images were independently reviewed by a second investigator. Any discrepancies in the evaluation or scoring were discussed between the evaluators until a final consensus was reached.

Wound healing and inflammation were assessed at a histological level using a modified scoring system based on DaCosta et al. (1998). The number of epithelial cells (Ep), fibroblasts (Fb), fibrocytes (Fc), collagen fibers (Cf), and vascular structures (Vc) per field was quantified and compared. A grading scale

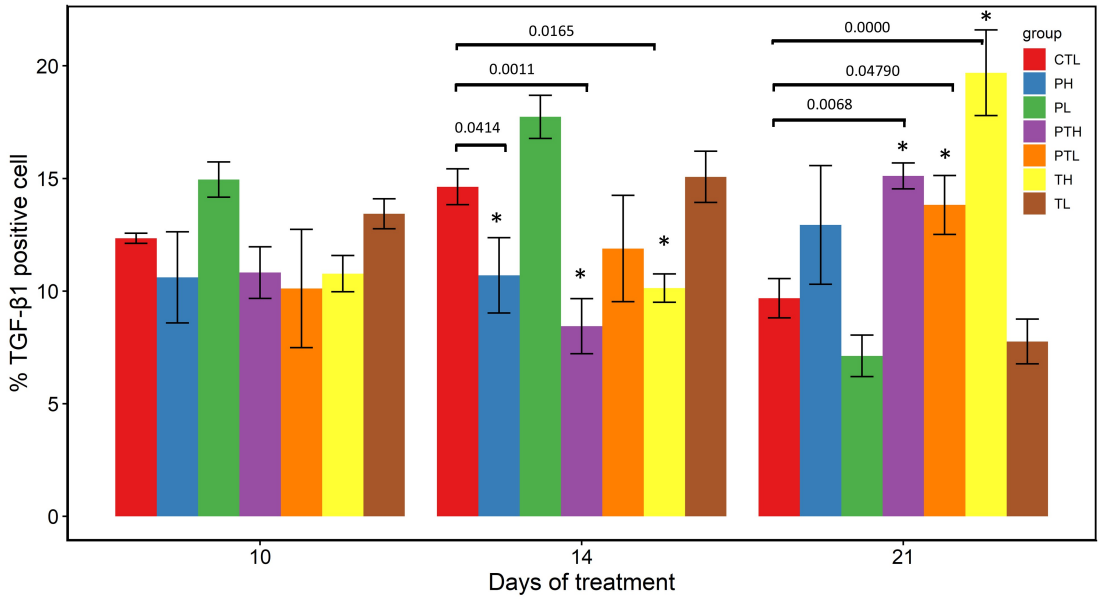

Figure 3. The TGF-β1 Levels in Wounds Treated with Each Formulation were Recorded on Days 10, 14, and 21. Data are Presented as Mean ± SD (n=3). *p < 0.05 vs Control. Brackets Indicate Adjusted p-Values for Significant Differences Between Treatment Groups and the Control on Specific Days

was used, with 1 indicating a few cells, 2 indicating a moderate presence, and 3 indicating an abundant presence.

Skin irritation was evaluated according to ISO 10993-6 guidelines (Siritientong et al., 2014), Infiltrations of polymorphonuclear cells (PMN), lymphocytes, plasma cells, macrophages, giant cells, necrosis, neovascularization, fibrosis, and fatty infiltrates were scored on a scale from 0 to 4 (0 = absent, 1 = rare, 2 = moderate, 3 = heavy infiltrate, and 4 = densely packed). The final irritation score was calculated using Equation (3):

$$\text{Final score} = [2I_t + N_t] - [2I_c + N_c] \quad (3)$$

I = Total number of inflammatory cells (t = test sample, c = control), and N = Total number of neovascularization, fibrosis, and fatty infiltrates (t = test sample, c = control) The irritation classification was as follows: 0.0 – 2.9 = No irritation, 3.0 – 8.9 = Slight irritation, 9.0 – 15 = Moderate irritation, and >15 = Severe irritation.

2.6 Immunohistochemistry Examination

The spatial expression of TGF-β1 was evaluated using an anti-mouse HRP-DAB Cell & Tissue Staining Kit. Tissue specimens were deparaffinized, rehydrated, and treated with a blocking reagent to inhibit endogenous enzyme activity for 15 minutes. The sections were then incubated with a mouse anti-TGF-β1 primary antibody at 1:25 dilution at 4 °C overnight. Following incubation, the slides were washed with phosphate-buffered saline (PBS) and subsequently incubated with a biotinylated secondary antibody for 60 minutes. High-sensitivity streptavidin-HRP (HSS-HRP) conjugate was then applied for 30 minutes. DAB (3,3-diaminobenzidine tetrahydrochloride) was used as the chromogen, producing a brown precipitate at immunopositive sites. The slides were counterstained with Harris's hematoxylin for contrast. The percentage of positive cells was quantified under an inverted microscope (Olympus DP73®, Olympus, San Diego, USA). The percentage of positive cells was calculated using Equation (4).

$$\text{Positive Cell (\%)} = \frac{\text{positive cell}}{(\text{normal cell} + \text{positive cell})} \times 100 \quad (4)$$

2.7 Statistical Analysis

The Shapiro-Wilk and Levene's tests were performed to assess normal distribution and homogeneity of variance, respectively. For variables that met parametric assumptions, ANOVA with Tukey's HSD post hoc test was used. For variables that did not follow a normal distribution, the non-parametric Kruskal-Wallis test followed by Dunn's test was applied. A p-value of less than 0.05 was considered statistically significant.

3. RESULTS AND DISCUSSIONS

3.1 Wound Contraction and Wound Histomorphology

The wound contraction data deviated from normal distributions and lacked equal variances. Thus, non-parametric Kruskal-Wallis with Dunn's test was performed. Figure 1 presents the progression of wound contraction for all groups over time. It indicated that the PTH, PTL, and TH groups showed a

trend toward faster wound contraction compared to the control group; however, these differences were not statistically significant. Early stages of wound contraction exhibited high variance, especially at day 3 to day 6. It may be explained by a well-documented physiological process. The wound bed may exhibit a heterogeneous biological transition from the inflammatory phase to the proliferative phase (Ozgok Kangal and Kopitnik, 2026). Additionally, naturally asymmetric contraction of the wounds also contributed to the increasing relative variability.

The PL group demonstrated a sharp increase in wound contraction across all groups from the 3rd to the 14th day, despite no statistical difference on day 3. This suggested that PL had a sustained, positive effect on the wound healing process. The effectiveness of PL hydrogel on wound healing was comparable to a recent study of Thymosin β4-Exosome loaded hydrogel, which achieved approximately 90% wound closure within 10 days (Yu et al., 2025). Additionally, the PH group exhibited significantly accelerated wound contraction on the 10th day. While the statistically significant improvements in this group were observed only at specific time points, these findings may suggest a transient therapeutic effect or a delayed onset of action. Conversely, a high dose of PAP appeared to exert its effects at a much later stage of the healing process. This behavior may be associated with concentration-dependent changes in macrophage responses. The role of macrophages in wound healing had been extensively documented, particularly during the inflammatory phase. Literature suggested a balance in macrophage activity as prolonged, excessive macrophage-mediated inflammation in the early phase can retard wound healing (Tao et al., 2025). In the later stages, macrophages contributed to angiogenesis, recruited fibroblasts, and activated fibroblasts to produce collagen (Khimmakthong et al., 2011; Yu et al., 2025). This aligned with a study that valproic acid accelerated skin wound healing by inhibiting the macrophage inflammatory response while enhancing macrophage phagocytic activity (Chen et al., 2023).

In the TL group, the wound area was significantly reduced compared to the control group on day 3 and from day 8 to day 14. Notably, the TL group achieved around 80% wound closure between days 6 and 8. These findings aligned with previous research by Altuntas et al. (2022) where epidermal growth factor (EGF)-doped nano chitosan–gelatin film significantly accelerated wound to 95 ± 12% between days 5 and 7. The close match between these outcomes implied that the EGF-like domain in TSP-3 exhibited biological activity comparable to that of native human growth factors (Chen et al., 2026).

Importantly, the PTH and TH hydrogel formulations containing a high dose of TSP exhibited inferior wound closure compared to the low-dose TSP formulations. This finding aligned with previous in vitro studies, which demonstrated that the optimal concentration of TSP for cell proliferation and collagen production is approximately 0.5 μg/mL, with higher concentrations leading to reduced activity (Wonglapsuwan et al., 2020). We hypothesize that continuous activation of the phagocytosis pathway could potentially alter the macrophages' behavior. It might indirectly affect extracellular matrix turnover regulation and retarded wound remodeling (Zheng et al., 2025). Additionally, although not confirmed by direct molecular data, overstimulation of epidermal growth factor receptors might be associated with altered receptor feedback loops.

Table 2. Wound Healing Score on Days 10, 14, and 21. Data are Presented as Median (n = 3)

Day	Treatment	Score				Total Score
		Ep	Fb & Fc	Cf	Vc	
	Normal tissue	3	4	3	1	11
10	CTL	1	4	1	2	8
	PL	2	4	1	2	9
	PH	1	4	1	2	8
	PTL	1	4	1	2	8
	TL	2	4	1	2	9
	TH	1	4	1	2	8
	PTH	1	4	1	1	7
14	CTL	2	4	1	2	9
	PL	3	4	2	2	11
	PH	2	4	2	2	10
	PTL	2	4	1	1	8
	TL	3	4	2	2	11
	TH	3	4	2	2	11
	PTH	2	4	2	2	10
21	CTL	3	4	2	2	11
	PL	3	4	2	2	11
	PH	3	4	2	2	11
	PTL	3	4	2	2	11
	TL	3	4	2	2	11
	TH	3	4	2	2	11
	PTH	3	4	2	2	11

* Ep = epithelial layer, Fb & Fc = fibroblast & fibrocyte, Cf = collagen fiber, Vc = vascular

3.2 Histological Studies

Histological analysis of wound healing and inflammation in each treatment group on days 10, 14, and 21 revealed minimal differences in overall wound healing scores (Table 2). This observation was consistent with the general timeline of the later stages of the wound healing process. By day 10, visible wound size across all groups had reduced to less than 25% of its original size, indicating substantial healing. Additionally, the epidermal thickness of most groups (CTL, TH, TL, and PTH) was significantly higher than the uninjured skin (Table 3) due to the wound may be transitioning from the proliferation phase, which had granulation tissue as a dominant characteristic toward the remodeling phase (Muñoz-Torres et al., 2025).

In contrast, the PL, PTL and PH groups showed no significant difference in epidermal thickness compared to normal skin.

Table 3. Epidermal and Dermal Thickness on Days 10, 14 and 24. Data are Presented as Mean ± SD (n = 12)

Day	Treatment	Epidermal Thickness			Dermal Thickness		
		Value (μm)	p-value		Value (μm)	p-value	
			to Normal Skin	to CTL		to Normal Skin	to CTL
Normal Skin		50.98±12.05	N/A	N/A	819.87±62.35	N/A	N/A
10	CTL	129.09±56.20	0.0023*	N/A	608.59±54.43	0.0111*	N/A
	PTL	51.95±12.44	0.9435	0.0029*	870.83±98.91	0.8327	0.0059*
	PH	78.14±31.70	0.1120	0.1447	846.48±82.88	0.9064	0.0079*
	TH	108.11±27.75	0.0038*	0.8789	626.46±56.67	0.0237*	0.7810
	PL	65.34±9.11	0.2008	0.0770*	596.47±42.66	0.0061*	0.8390
	TL	122.70±35.73	0.0015*	0.8937	687.71±58.05	0.1985	0.2099
	PTH	101.80±36.60	0.0143*	0.5502	673.19±57.24	0.1242	0.3161
14	CTL	64.03±11.15	0.2576	N/A	466.38±34.47	<0.0001*	N/A
	PTL	74.43±20.39	0.1018	0.6143	493.91±26.60	<0.0001*	0.6022
	PH	66.11±30.44	0.4904	0.6582	727.58±106.05	0.3084	0.0000
	TH	30.65±6.90	0.0081*	0.0002*	468.58±38.88	<0.0001*	0.9638
	PL	44.53±12.46	0.4878	0.0679	638.33±69.60	0.0435*	0.0014
	TL	35.35±8.53	0.0516*	0.0021*	447.41±21.45	<0.0001*	0.6806
	PTH	41.89±10.78	0.2959	0.0294*	547.03±42.02	0.0002*	0.1262
21	CTL	34.71±10.23	0.0369*	N/A	541.18±101.38	0.0001*	N/A
	PTL	27.37±4.27	0.0016*	0.2831	351.57±42.83	<0.0001*	0.0015*
	PH	32.57±9.98	0.0178	0.7769	591.44±85.00	0.0038*	0.3550
	TH	25.47±13.85	0.0006*	0.1766	357.29±72.12	<0.0001*	0.0031*
	PL	43.40±11.90	0.3494	0.2498	406.02±58.82	<0.0001*	0.0162*
	TL	29.94±8.10	0.0075*	0.5564	502.84±67.43	<0.0001*	0.4837
	PTH	30.72±7.22	0.0074*	0.5546	369.03±38.11	<0.0001*	0.0024*

* $p<0.05$

The epidermal layers, including the stratum basale, stratum spinosum, and stratum corneum, were quite well-defined and fully developed. Within these tissues, populations of fibroblasts, fibrocytes, and neocapillaries were abundant. Inflammatory cells were absent in the wound area at this stage, which was consistent with the anticipated timetable of the inflammatory process, which generally occurs within the initial days following damage (Figure 2A). Additionally, epithelial cell connectivity in the PL groups was significantly more intact than in the other groups. This implied that PL, PTL and PH shifted to the remodeling phase earlier than other treatments. The dermal thickness of all groups was close to normal baseline values. This result confirmed that the effectiveness of hydrogel could promote rapid proliferation of the dermal layer (Pan et al., 2025).

By the second week, the similarity in histological scores across treatments may indicate that collagen maturation and initial tissue remodeling followed a consistent pattern. The overall wound healing score gradually increased. This slight improvement appeared to be contributed by epithelialization and collagen fiber deposition score. The PL, TL, and TH groups achieved the highest scores of 11 (Table 2), with epithelial cell connections that were nearly complete, whereas the PH, PTL, and PTH groups showed no marked difference compared to the control (Figure 2B). Collagen fiber deposition scores showed a slight upward trend in the treatment groups compared to the control, except in the PTL group, where the score remained unchanged from day 10.

On day 21, the wound healing score of all groups had reached levels comparable to those of normal tissue, indicating that the healing process was nearly complete. The morphological characteristics resembled those of normal tissue, with minimal new vascularization. The thickness of the epidermal layer was nearly identical to that of healthy skin (Figure 2C). The epidermal thickness from day 14 onward significantly decreased to normal (±50 μm), especially in the PL group that returned to normal earlier (Table 3) and aligned with wound healing score and wound contraction data. On the other hand, the dermal thickness continued to be thinner than the normal skin from day 14. This phenomenon may be attributed to the active contraction of the wound edge by myofibroblasts, which reduced the defect size (Liu et al., 2025).

Skin irritation score yielded non-normally distributed data, which was analyzed using Kruskal-Wallis and Dunn's tests. The analysis showed no significant differences in inflammatory cell presence, neovascularization, fibrosis, or fat infiltration compared to normal skin tissue. The total irritation score for wounds treated with hydrogel, across all seven formulations, remained below 2 on days 10, 14, and 21 (Table 4). Additionally, no signs of skin irritation were observed in the wound area, particularly on days 14 and 21, when inflammation had completely resolved. These findings indicate that neither the

Table 4. Skin Irritation Score on Days 10, 14, and 21. Data are Presented as Mean ± SD (n=5)

Day	Treatment	Neutrophil	Lymphocyte	Plasma Cell	Macrophage	Giant Cell	Debris	Neovascularize	Fibrosis	Fat Infiltration	Irritation Score	p-Value
		Cells/Field						Occurrences /Field				
10	CTL	0.00 ± 0.00	0.00 ± 0.00	0.00 ± 0.00	0.00 ± 0.00	0.00 ± 0.00	0.00 ± 0.00	2.80 ± 0.79	0.00 ± 0.00	0.00 ± 0.00	1.24 ± 0.95	
	PL	0.00 ± 0.00	0.40 ± 0.55	0.00 ± 0.00	0.00 ± 0.00	0.00 ± 0.00	0.00 ± 0.00	3.20 ± 0.55	0.00 ± 0.00	0.00 ± 0.00	2.14 ± 0.84	
	PH	0.00 ± 0.00	0.00 ± 0.00	0.00 ± 0.00	0.00 ± 0.00	0.00 ± 0.00	0.00 ± 0.00	3.40 ± 0.55	0.00 ± 0.00	0.00 ± 0.00	1.54 ± 0.55	
	PTL	0.00 ± 0.00	0.00 ± 0.00	0.20 ± 0.45	0.00 ± 0.00	0.00 ± 0.00	0.00 ± 0.00	2.80 ± 0.55	0.00 ± 0.00	0.00 ± 0.00	1.74 ± 1.30	0.3640
	TL	0.20 ± 0.45	0.00 ± 0.00	0.00 ± 0.00	0.00 ± 0.00	0.00 ± 0.00	0.00 ± 0.00	2.80 ± 0.45	0.00 ± 0.00	0.00 ± 0.00	1.74 ± 0.84	
	TH	0.00 ± 0.00	0.00 ± 0.00	0.00 ± 0.00	0.00 ± 0.00	0.00 ± 0.00	0.00 ± 0.00	3.40 ± 0.55	0.00 ± 0.00	0.00 ± 0.00	1.14 ± 0.45	
	PTH	0.00 ± 0.00	0.00 ± 0.00	0.20 ± 0.45	0.00 ± 0.00	0.00 ± 0.00	0.00 ± 0.00	2.80 ± 0.55	0.00 ± 0.00	0.00 ± 0.00	1.14 ± 0.45	
14	CTL	0.00 ± 0.00	0.00 ± 0.00	0.00 ± 0.00	0.00 ± 0.00	0.11 ± 0.33	0.11 ± 0.33	2.78 ± 0.50	0.00 ± 0.00	0.00 ± 0.00	1.50 ± 1.01	
	PL	0.00 ± 0.00	0.00 ± 0.00	0.00 ± 0.00	0.00 ± 0.00	0.00 ± 0.00	0.00 ± 0.00	3.20 ± 0.45	0.00 ± 0.00	0.00 ± 0.00	1.14 ± 0.45	
	PH	0.00 ± 0.00	0.00 ± 0.00	0.00 ± 0.00	0.00 ± 0.00	0.00 ± 0.00	0.00 ± 0.00	2.60 ± 0.45	0.00 ± 0.00	0.00 ± 0.00	1.14 ± 0.45	
	PTL	0.00 ± 0.00	0.00 ± 0.00	0.00 ± 0.00	0.00 ± 0.00	0.00 ± 0.00	0.00 ± 0.00	2.80 ± 0.45	0.00 ± 0.00	0.00 ± 0.00	1.14 ± 0.45	0.6890
	TL	0.00 ± 0.00	0.00 ± 0.00	0.00 ± 0.00	0.00 ± 0.00	0.00 ± 0.00	0.00 ± 0.00	3.25 ± 0.58	0.00 ± 0.00	0.00 ± 0.00	1.44 ± 0.58	
	TH	0.00 ± 0.00	0.00 ± 0.00	0.00 ± 0.00	0.00 ± 0.00	0.00 ± 0.00	0.00 ± 0.00	2.75 ± 0.58	0.00 ± 0.00	0.00 ± 0.00	1.44 ± 0.58	
	PTH	0.00 ± 0.00	0.00 ± 0.00	0.00 ± 0.00	0.00 ± 0.00	0.00 ± 0.00	0.00 ± 0.00	2.25 ± 0.00	0.00 ± 0.00	0.00 ± 0.00	0.94 ± 0.00	
21	CTL	0.00 ± 0.00	0.00 ± 0.00	0.00 ± 0.00	0.00 ± 0.00	0.00 ± 0.00	0.00 ± 0.00	2.22 ± 0.33	0.00 ± 0.00	0.00 ± 0.00	1.05 ± 0.33	
	PL	0.00 ± 0.00	0.00 ± 0.00	0.00 ± 0.00	0.00 ± 0.00	0.00 ± 0.00	0.00 ± 0.00	3.00 ± 0.45	0.00 ± 0.00	0.00 ± 0.00	1.14 ± 0.45	
	PH	0.00 ± 0.00	0.00 ± 0.00	0.00 ± 0.00	0.00 ± 0.00	0.00 ± 0.00	0.00 ± 0.00	2.80 ± 0.45	0.00 ± 0.00	0.00 ± 0.00	1.14 ± 0.45	
	PTL	0.00 ± 0.00	0.00 ± 0.00	0.00 ± 0.00	0.00 ± 0.00	0.00 ± 0.00	0.00 ± 0.00	2.60 ± 0.45	0.00 ± 0.00	0.00 ± 0.00	1.14 ± 0.45	0.6060
	TL	0.00 ± 0.00	0.00 ± 0.00	0.00 ± 0.00	0.00 ± 0.00	0.00 ± 0.00	0.00 ± 0.00	3.25 ± 0.58	0.00 ± 0.00	0.00 ± 0.00	1.44 ± 0.58	
	TH	0.00 ± 0.00	0.00 ± 0.00	0.00 ± 0.00	0.00 ± 0.00	0.00 ± 0.00	0.00 ± 0.00	3.50 ± 0.58	0.00 ± 0.00	0.00 ± 0.00	1.44 ± 0.58	
	PTH	0.00 ± 0.00	0.00 ± 0.00	0.00 ± 0.00	0.00 ± 0.00	0.00 ± 0.00	0.00 ± 0.00	3.25 ± 0.58	0.00 ± 0.00	0.00 ± 0.00	1.44 ± 0.58	

hydrogel base nor the formulations containing PAP and TSP caused skin irritation.

3.3 Expression of TGF-β1

Since the quantitative immunohistochemical datasets followed normal distributions with homogeneous variances, parametric ANOVA and Tukey's HSD post-hoc tests were performed. Figure 3 shows the TGF-β1 levels for each group over time. In this study, the TGF-β1 had biphasic dose-response characteristics. Low dose of PAP and TSP in TL and PL group followed the normal pattern of TGF-β1 by rising during the early- to mid-stages of wound healing and subsiding in the later phases (Pakyari et al., 2013). TGF-β1 expression in the PL group peaked considerably on day 14 (17.73 ± 0.94%) and was closely followed by the TL group (15.07 ± 0.94%). This result was aligned with the wound contraction where the PL group had the best wound reduction. Notably, both the PL and TL groups demonstrated a sharp and highly consistent downregulation by day 21, dropping to 7.12 ± 0.92% and 7.76 ± 0.53%, respectively, falling below the control baseline (9.68 ± 0.84%). These incidents perfectly mimicked the natural physiological process for ideal, scarless tissue repair. The peak of TGF-β1 observed at day 14 could be interpreted as the end of the early inflammatory phase, which the literature frequently associates with shifts in macrophage-driven inflammation (He et al., 2026; Sun et al., 2026).

In contrast, high doses of either PAP or TSP, including PH, TH, and the combined PTH group failed to elevate TGF-β1 at the beginning of the proliferation stage of wound healing. The PTH group exhibited the lowest expression at this time point (8.44 ± 0.61%). However, the high-dose groups exhibited a delayed surge in TGF-β1 expression by day 21. The TH and PTH groups reached peaks of 19.69 ± 1.54% and 15.12 ± 1.05%, respectively. Moreover, a slight increase in TGF-β1 levels was also observed in the TL group, likely due to the EGF-like domain of TSP, which promotes cell proliferation without much interferance with the natural feedback loop (Sweetwyne and Murphy-Ullrich, 2012). The significant decrease in TGF-β1 levels during the late phase of wound healing suggested proper wound progression, consistent with prior studies (Franz, 2015; Huang and Fu, 2015; Pakyari et al., 2013).

The interesting trend in this study was that the high-dose groups (PH, TH, and PTH) statistically significantly (p-value = 0.041, 0.001 and 0.017, respectively) exhibited paradoxical under-effectiveness during the day 14 proliferative window. While PAP and TSP were reported as potent activators of TGF-β1-releasing cells, the data tend to follow a non-linear, biphasic dose-response curve. However, the precise mechanism behind this biphasic dose-response phenomenon was still largely hypothetical and unsupported by direct molecular evidence in this study. We hypothesized that high concentrations of these compounds might stimulate receptors and potentially lead to rapid receptor internalization and downregulation (Xie et al., 2025). Alternatively, the macrophages might remain in an inflammatory state, delaying the biological clock of the wound. Consequently, the TGF-β1 levels were suppressed as observed at days 10 and 14. In addition, previous studies have demonstrated that the overactivation of fibroblasts and keratinocytes upregulates Smad3 and Smad4, subsequently leading to the activation of Smad7. Smad7 essentially acts as a brake to stabilize TGF-β1 levels (Miyazono, 2000). Because parameters like Smad signaling, macrophage polarization markers, and receptor internalization were not directly evaluated in this study, these mechanistic explanations remain entirely speculative.

The delayed surge of TGF-β1 in the PTL, PTH and TH groups compared to the control group at day 21 may reflect gradual recovery of receptor or altered temporal signaling dynamics (von Zastrow and Sorkin, 2021). However, this late-

stage elevation warranted attention as prolonged or delayed TGF-β1 surges may increase the risk of subsequent scar formation (Bonnici et al., 2024).

This study has some limitations. By incising four wounds on each animal, we can ethically reduce the total number of animals used while also minimizing natural variations between individuals. We acknowledge that the four wounds on a single subject share the same systemic biological and immunological environment, meaning strict statistical independence between these specific wound sites cannot be absolute. However, given the localized, topical nature of the hydrogel application and the sufficient physical spacing of the treatment sites, systemic absorption and subsequent pharmacological cross-site interference are anticipated to be negligible. The small sample size of histology and TGF-β1 immunohistology evaluation may contribute to the high variation and limit the interpretation of results.

4. CONCLUSIONS

Although the physicochemical properties and drug release profile were not fully characterized. The safety and efficacy of seven different hydrogel formulations were evaluated in rats, with no skin irritation observed. Among these, the hydrogel containing a low dose of PAP demonstrated the highest wound contraction rate, favorable histological characteristics of wound healing, and elevated TGF-β1 levels. The hydrogel with a low TSP dose also exhibited strong wound-healing properties, closely matching PAP in effectiveness. These findings suggest that hydrogels containing PAP and TSP hold significant potential as wound-healing therapies. Therefore, formulations with low doses of PAP or TSP could serve as promising candidates for the development of advanced wound dressings with controlled-release properties. However, further molecular-level investigations are required to better understand the underlying mechanisms driving their efficacy.

5. ACKNOWLEDGEMENT

This work was funded by the Prince of Songkla University Super Cluster Grant, Grant No. 2560IA1150020. The authors extend their sincere gratitude to Mr. Nattharit Roekngam for his valuable assistance in this research.

REFERENCES

Acciaretti, F., S. Vesentini, and L. Cipolla (2022). Fabrication Strategies Towards Hydrogels for Biomedical Application: Chemical and Mechanical Insights. *Chemistry–An Asian Journal*, **17**(22); e202200797

Altuntas, S., H. K. Dhaliwal, A. Eid Radwan, M. Amiji, and F. Buyukserin (2022). Local Epidermal Growth Factor Delivery Using Nanopillared Chitosan–Gelatin Films for Melanogenesis and Wound Healing. *Biomaterials Science*, **11**(1); 181–194

Aramwit, P. and A. Sangcakul (2007). The Effects of Sericin Cream on Wound Healing in Rats. *Bioscience, Biotechnology, and Biochemistry*, **71**(10); 2473–2477

Bogadi, S., M. E. Uddin, M. H. Rahman, V. V. S. R. Karri, R. Begum, and S. E. Udeabor (2025). Wound Healing in the Modern Era: Emerging Research, Biomedical Advances, and Transformative Clinical Approaches. *Journal of Drug Delivery Science and Technology*, **110**; 107058

Bonnici, L., S. Suleiman, P. Schembri-Wismayer, and A. Cassar (2024). Targeting Signalling Pathways in Chronic Wound Healing. *International Journal of Molecular Sciences*, **25**(1); 50

Chen, H., F. Liang, C. Fu, Z. Wang, and Z. Zhang (2023). Valproic Acid Accelerates Skin Wound Healing in Mice Via Its Anti-Inflammatory and Apoptotic Cell Clearance-Promoting Effects. *Journal of International Medical Research*, **51**(6); 03000605231184038

Chen, L.-s., B.-w. Zheng, C.-y. Zhao, C.-c. He, and X.-H. Gao (2026). The Role of Thrombospondin-1 in Dermatological Conditions. *Frontiers in Medicine*, **13**; 1724955

DaCosta, M. L., M. C. Regan, M. Al Sader, M. Leader, and D. Bouchier-Hayes (1998). Diphenylhydantoin Sodium Promotes Early and Marked Angiogenesis and Results in Increased Collagen Deposition and Tensile Strength in Healing Wounds. *Surgery*, **123**(3); 287–293

Deachamag, P., U. Intaraphad, A. Phongdara, and W. Chotigeat (2006). Expression of a Phagocytosis Activating Protein (PAP) Gene in Immunized Black Tiger Shrimp. *Aquaculture*, **255**(1–4); 165–172

Franz, M. G. (2015). Wound Healing. In G. M. Doherty, editor, *CURRENT Diagnosis & Treatment: Surgery*. McGraw-Hill Education, New York, NY, 14 edition

Grellner, W., S. Vieler, and B. Madea (2005). Transforming Growth Factors (TGF-α and TGF-β1) in the Determination of Vitality and Wound Age: Immunohistochemical Study on Human Skin Wounds. *Forensic Science International*, **153**(2); 174–180

Guo, S. and L. A. DiPietro (2010). Factors Affecting Wound Healing. *Journal of Dental Research*, **89**(3); 219–229

He, X., W. Wu, Y. Hu, M. Wu, H. Li, L. Ding, S. Huang, and Y. Fan (2024). Visualizing the Global Trends of Peptides in Wound Healing through an In-Depth Bibliometric Analysis. *International Wound Journal*, **21**(4); e14575

He, Y., J. Hu, A. Ma, P. Du, M. Yang, X. Xiong, and Y. Deng (2026). The Crosstalk Between Efferocytosis and Macrophage Polarization in Diabetic Wounds: A Comprehensive Review. *Journal of Inflammation Research*; 566523

Huang, L. and L. Fu (2015). Mechanisms of Resistance to EGFR Tyrosine Kinase Inhibitors. *Acta Pharmaceutica Sinica B*, **5**(5); 390–401

Kamlungmak, S., J. Dechraksa, A. R. Padmavathi, S. Sawatdee, K. Tinpun, T. Nakpheng, and T. Srichana (2019). Lamellar Phase Behavior and Molecular Interaction of a Thermoresponsive Poloxamer and Crosslinked Poly(Vinyl Alcohol) Hydrogel. *Materials Today Communications*, **20**; 100542

Kamlungmak, S., T. Nakpheng, S. Kaewpaiboon, M. A. K. M. Bintang, S. Prom-In, C. Chunhachaichana, and

T. Srichana (2021). Safety and Biocompatibility of Mupirocin Nanoparticle-Loaded Hydrogel on Burn Wound in Rat Model. *Biological and Pharmaceutical Bulletin*, **44**(11); 1707–1716

Khimmakthong, U., P. Deachamag, A. Phongdara, and W. Chotigeat (2011). Stimulating the Immune Response of *Litopenaeus vannamei* Using the Phagocytosis Activating Protein (PAP) Gene. *Fish & Shellfish Immunology*, **31**(3); 415–422

Koh, T. J. and L. A. DiPietro (2011). Inflammation and Wound Healing: The Role of the Macrophage. *Expert Reviews in Molecular Medicine*, **13**; e23

Kohyama, K., H. Kato, H. Okada, T. Ishihara, Y. Yasue, R. Kamidani, K. Suzuki, T. Miyake, H. Okuda, H. Shibata, et al. (2024). Concomitant Heparin Use Promotes Skin Graft Donor Site Healing by Basic Fibroblast Growth Factor: A Pilot Prospective Randomized Controlled Study. *Contemporary Clinical Trials Communications*, **42**; 101375

Larouche, J., S. Sheoran, K. Maruyama, and M. M. Martino (2018). Immune Regulation of Skin Wound Healing: Mechanisms and Novel Therapeutic Targets. *Advances in Wound Care*, **7**(7); 209–231

Liu, A., P. Garg, S. Yang, P. Gong, M. A. Pallero, D. S. Annis, J. E. Murphy-Ullrich, and S. E. Goldblum (2009). Epidermal Growth Factor-Like Repeats of Thrombospondins Activate Phospholipase Cγ and Increase Epithelial Cell Migration Through Indirect Epidermal Growth Factor Receptor Activation. *Journal of Biological Chemistry*, **284**(10); 6389–6402

Liu, Z., L. Chen, B. Hao, Y. Hou, C. Lv, Y. Zhu, and C. Han (2025). SHP099-Containing Multi-Targeting Hydrogel Promotes Rapid Skin Reconstruction Through Modulating a Variety of Cells. *Frontiers in Bioengineering and Biotechnology*, **13**; 1564827

Lowe, J. M., D. Menendez, and M. B. Fessler (2014). A New Inflammatory Role for p53 in Human Macrophages. *Cell Cycle*, **13**(19); 2983–2984

Mârza, S. M., A. M. Dăescu, R. C. Purdoiu, M. Dragomir, M. Tătaru, I. Melega, and I. Papuc (2024). Healing of Skin Wounds in Rats Using Creams Based on *Symphytum officinale* Extract. *International Journal of Molecular Sciences*, **25**(6); 3099

Miyazono, K. (2000). Positive and Negative Regulation of TGF-β Signaling. *Journal of Cell Science*, **113**(7); 1101–1109

Muñoz-Torres, J. R., I. Garza-Veloz, P. Velasco-Elizondo, and M. L. Martinez-Fierro (2025). HEALS-A and GRADES: Novel Histological and Clinical Scales for Assessing Skin Regeneration in Murine Wound Healing Models. *Diagnostics*, **15**(3); 387

Ozgok Kangal, M. K. and N. L. Kopitnik (2026). Physiology, Wound Healing. In *StatPearls*. StatPearls Publishing, Treasure Island, FL

Pakyari, M., A. Farrokhi, M. K. Maharlooei, and A. Ghahary (2013). Critical Role of Transforming Growth Factor Beta in Different Phases of Wound Healing. *Advances in Wound Care*, **2**(5); 215–224

Pan, Y., Y. Li, X. Zhou, J. Luo, Q. Ding, R. Pan, and X. Tian (2025). Extracellular Matrix-Mimicking Hydrogel with Angiogenic and Immunomodulatory Properties Accelerates Healing of Diabetic Wounds by Promoting Autophagy. *ACS Applied Materials & Interfaces*, **17**(3); 4608–4625

Sari, M. H. M., A. d. F. Cobre, R. Pontarolo, and L. M. Ferreira (2023). Status and Future Scope of Soft Nanoparticles-Based Hydrogel in Wound Healing. *Pharmaceutics*, **15**(3); 874

Shekhar, M., M. DilliKumar, K. Vinaya Kumar, G. Gopikrishna, S. Rajesh, J. Kiruthika, and A. Ponniah (2012). Transcript Analysis of White Spot Syndrome Virus Latency and Phagocytosis Activating Protein Genes in Infected Shrimp (*Penaeus monodon*). *Indian Journal of Virology*, **23**(3); 333–343

Siritientong, T., A. Angspatt, J. Ratanavaraporn, and P. Aramwit (2014). Clinical Potential of a Silk Sericin-Releasing Bioactive Wound Dressing for the Treatment of Split-Thickness Skin Graft Donor Sites. *Pharmaceutical Research*, **31**(1); 104–116

Smith, J. and V. Rai (2024). Novel Factors Regulating Proliferation, Migration, and Differentiation of Fibroblasts, Keratinocytes, and Vascular Smooth Muscle Cells During Wound Healing. *Biomedicines*, **12**(9); 1939

Sun, Y., H. Guo, Y. Bai, J. Chen, and Y. Li (2026). Roles of Efferocytosis in Wound Repair: Process, Cells, and Signals. *Genes & Diseases*, **13**(3); 101937

Sweetwyne, M. T. and J. E. Murphy-Ullrich (2012). Thrombospondin-1 in Tissue Repair and Fibrosis: TGF-β-Dependent and Independent Mechanisms. *Matrix Biology*, **31**(3); 178–186

Tao, L., S. Wu, Q. Wang, Z. Xi, Y. Zou, M. Cao, K. Liang, W. Xu, Q. Hu, Y. Ge, et al. (2025). IL-27 Accelerates Diabetic Wound Healing by Modulating Macrophage Polarization. *International Immunopharmacology*, **155**; 114575

Terzian, T. and G. Lozano (2010). Building p53. *Genes & Development*, **24**(20); 2229–2232

von Zastrow, M. and A. Sorkin (2021). Mechanisms for Regulating and Organizing Receptor Signaling by Endocytosis. *Annual Review of Biochemistry*, **90**; 709–737

Widowati, W., D. Rahmat, A. Faried, I. M. Nainggolan, D. Priyandoko, T. L. Wargasetia, and J. Jeffrey (2025). Potential of Secretome Hydrogel for Wound Healing in LPS- and Scratch-Induced BJ Cells as an Inflammation Model. *Science and Technology Indonesia*, **10**(4); 1242–1254

Wonglapsuwan, M., N. Khwanmuang, P. Deachamag, and W. Chotigeat (2020). Biological Activity of the Thrombospondin Epidermal Growth Factor Domain from Banana Shrimp (*Fenneropenaeus merguiensis*). *ScienceAsia*, **46S**(1); 27–35

Wonglapsuwan, M., P. Kongmee, N. Suanyuk, and W. Chotigeat (2016). Roles of Phagocytosis Activating Protein (PAP) in *Aeromonas hydrophila*-Infected *Cyprinus carpio*. *Developmental and Comparative Immunology*, **59**; 25–33

Xie, Y., Z. Wu, J. Wang, Z. Li, and Z. Hu (2025). Dissolvable

Core–Shell Microneedle Patch for Biphasic Drug Delivery to Enhance Diabetic Wound Healing. *ACS Applied Materials & Interfaces*, **17**(17); 25152–25162

Yu, H., B. Wang, Z. Li, K. Liu, W. Chen, S. Zhao, and L. Li (2025). Tβ4-Exosome-Loaded Hemostatic and Antibacterial Hydrogel to Improve Vascular Regeneration and Modulate Macrophage Polarization for Diabetic Wound Treatment. *Materials Today Bio*, **31**; 101585

Zhang, P. and C. Liu (2020). Enhancement of Skin Wound Healing by rhEGF-Loaded Carboxymethyl Chitosan Nanoparticles. *Polymers*, **12**(7); 1612

Zhang, Y., X. Liu, J. Zhao, J. Wang, Q. Song, and C. Zhao (2022). The Phagocytic Receptors of β-Glucan. *International Journal of Biological Macromolecules*, **205**; 430–441

Zhao, Y., L. Huang, G. Lin, M. Tong, Y. Xie, H. Pan, and H. Xu (2022). Skin-Adaptive Film Dressing with Smart-Release of Growth Factors Accelerated Diabetic Wound Healing. *International Journal of Biological Macromolecules*, **222**; 2729–2743

Zhao, Y., M. Li, J. Mao, Y. Su, X. Huang, W. Xia, and T. Zan (2024). Immunomodulation of Wound Healing Leading to Efferocytosis. *Smart Medicine*, **3**(1); e20230036

Zheng, Y., Z. Ruan, S. Liu, X. Yang, and Z. Chen (2025). Exosome-Mediated Macrophage Polarization: Pioneering Pathways in Diabetic Wound Healing. *International Immunopharmacology*, **161**; 115058

